Engineering 48 (2025) 309–322

Contents lists available at ScienceDirect

Engineering

journal homepage: www.elsevier.com/locate/eng

Research
Engineering Management—Article

Future Ultrafast Charging Stations for Electric Vehicles in China: Charging Patterns, Grid Impacts and Solutions, and Upgrade Costs

Yang Zhao [a,b], Xinyu Chen [a,*], Peng Liu [c], Chris P. Nielsen [b], Michael B. McElroy [b,d,*]

[a] School of Electrical Engineering, Huazhong University of Science and Technology, Wuhan 430074, China
[b] Harvard–China Project on Energy, Economy and Environment, Harvard John A. Paulson School of Engineering and Applied Sciences, Harvard University, Cambridge, MA 02138, USA
[c] National Engineering Research Center of Electric Vehicles, Beijing Institute of Technology, Beijing 100081, China
[d] Department of Earth and Planetary Sciences, Harvard University, Cambridge, MA 02138, USA

ARTICLE INFO

Article history:
Received 29 July 2024
Revised 17 December 2024
Accepted 15 January 2025
Available online 22 February 2025

Keywords:
Electric vehicle
Ultrafast charging
Grid impact
Charging infrastructure
Upgrade cost

ABSTRACT

In China, electric vehicle (EV) fast-charging power has quadrupled in the past five years, progressing toward 10-minute ultrafast charging. This rapid increase raises concerns about the impact on the power grid including increased peak power demand and the need for substantial upgrades to power infrastructure. Here, we introduce an integrated model to assess fast and ultrafast charging impacts for representative charging stations in China, combining real-world charging patterns and detailed station optimization models. We find that larger stations with 12 or more chargers experience modest peak power increases of less than 30% when fast-charging power is doubled, primarily because shorter charging sessions are less likely to overlap. For more typical stations (e.g., 8–9 chargers and 120 kW·charger^{-1}), upgrading chargers to 350–550 kW while allowing managed dynamic waiting strategies (of ~1 minute) can reduce overall charging times to ~9 minutes. At stations, deploying battery storage and/or expanding transformers can help manage future increases in station loads, yet the primary device cost of the former is ~4 times higher than that of the latter. Our results offer insights for charging infrastructure planning, EV–grid interactions, and associated policymaking.

1. Introduction

The global stock of electric vehicles (EVs) surpassed 40 million in 2023 [1]. The annual global sales of EVs increased at a nearly exponential rate over the past 4 years: 3 million in 2020, 6.6 million in 2021, 10.5 million in 2022, and 14 million in 2023 [1–4]. According to recent projections, the global stock of EVs would need to increase to 525 million in 2035 to meet current policy plans [1]. Among jurisdictions worldwide, China has the largest EV market in the world. Its EV stock, comprising battery EVs and plug-in hybrid EVs, exceeded 21 million in 2023 [1], which was over half of the global inventory for that year. Playing a critical role in strategies to achieve carbon neutrality, EVs will maintain a fast-growing trend while potentially offering more flexible power demands that could aid grid accommodation of variable renewable power generation [5].

Widespread EV deployment poses challenges for charging infrastructure. To alleviate pressure on charging accessibility, China has expanded its charging infrastructure to 11.4 million chargers (including 3.3 million public chargers) by September 2024, achieving a ratio of one charger for every ~2.5 EVs [6]. Importantly, the charging power of EVs has been rising significantly in recent years. The increases in both EV charging power and numbers of charging facilities could pose challenges for regional power systems. In this context, more investigation is needed of the intersection of charging behavior of EVs and charging stations as power levels rise, the resulting impacts on the grid, and the costs of potential solutions.

Fast charging of EVs conventionally refers to direct current (DC) charging at a power of 30 kW or above, as is increasingly deployed. Ultrafast charging, also called extreme fast charging, is a less standardized term for a type of fast charging. It refers to speeds of EV charging comparable to that of refueling gasoline or diesel cars,

* Corresponding authors.
E-mail addresses: xchen2019@hust.edu.cn (X. Chen), mbm@seas.harvard.edu (M.B. McElroy).

https://doi.org/10.1016/j.eng.2025.01.015

generally understood as 10 minutes or less [7,8]. Typically, EV ultrafast charging depends on two factors: whether it can accept high charging current rates, and whether the charging facilities can provide the high-power input. For batteries, studies of ultrafast charging prevailed much earlier than deployment for actual vehicles [9]. The main obstacles to fast-charging batteries concern insufficient electrolyte transport properties and cathode particle cracking [8]. An ultrafast 10-minute charge usually needs a charging current rate equal to or higher than 6C (the C-rate is a standard measure of charge/discharge rates relative to battery capacity). Significant progress on this front has been achieved. For instance, Lu et al. [10] demonstrated the design of a novel structure in the graphite anode for lithium-ion batteries, which could realize a state-of-charge (SOC) increase of 60% in 6 minutes (at a charging current rate of 6C). Ye and Li [11] presented a solid-state battery design with Li metal anodes, NMC811 cathodes, and multilayer electrolytes. With this configuration, the capacity of the battery could retain a charge of 82% after 10 000 cycles at a 20C charging rate. Driven by growing demand in EV markets, fast-charging technologies will continue to undergo rapid development. For vehicles, the fast-charging power of EVs sold in China has increased up to 4-fold from 30–120 to 60–480 kW over the past 5 years [12-14]. The fast-charging power of Tesla electric cars (e.g., Model 3) reaches 250 kW (Supercharger V3) and is planned to be upgraded further to 500 kW [15,16]. The Porsche Taycan achieves a maximum fast-charging power of 270 kW such that the 93-kW·h battery can be recharged from 10% to 80% in 19 minutes [17]. GAC AION EVs offered a 6C fast-charging option with a maximum power of 480 kW, sufficient to raise the battery SOC from 30% to 80% in 5 minutes [18]. Vehicle-side charging research also focuses on battery management systems (BMS), which monitor and control battery activities; important considerations include fast-charging protocols [19,20] and thermal management [21,22]. On the facility side, chargers are used to provide dynamic voltages and currents required by BMSs during EV charging processes. In China, state-of-the-art DC fast chargers in charging stations usually take a three-phase alternating current (AC) voltage between 380–480 V as an input and output a DC voltage between 200–1000 V [23]. To raise power levels and reduce cable weight, EV battery voltages are elevated from 400 to 800 V [24]. Based on high-voltage protocols, up-to-date deployed DC ultrafast chargers can provide maximum power of up to 600 kW [25]. Although such ultrafast EV charging technologies have developed dramatically over recent years, comparable charging stations have not yet been widely deployed.

Challenges remain in promoting EV ultrafast charging stations. First, the concurrent operation of several ultrafast chargers can easily be responsible for megawatt-level peak power demand, raising subsequent pressure to power infrastructure. Second, upgrading to ultrafast charging stations has a high investment cost. Third, the rapid development of ultrafast charging technologies may force repeated upgrades of charging stations. Existing studies have contributed greatly to addressing these challenges. Ahmad et al. [26] suggested that directly connecting ultrafast charging infrastructure to medium-voltage grids could help overcome the vulnerability of low-voltage distribution systems. Meyer and Wang [27] indicated that better location and capacity planning for ultrafast charging stations is important for mitigating negative impacts on power infrastructure. Fang et al. [28] presented a dynamic pricing scheme for fast-charging sharing systems to alleviate the shortage of fast-charging stations. Some research also links EV ultrafast charging research with popular related topics, for instance, smart cities [27], photovoltaics and energy storage [29,30], and microgrid scheduling [31,32]. However, research gaps remain in current studies. First, their use of real-world data is limited: Most studies rely on macroscopic simulations with designated parameters rather than actual EV use patterns, leading to potential biases that make the findings less applicable to real-world conditions. Second, they leave the relationship between EV charging power and station peak loads unclear: There is insufficient understanding of how increases in EV charging power affect the overall peak load on charging stations, which complicates accurate grid impact predictions. Third, they lack comparative analysis of upgrade strategies: There is a need for more research comparing different strategies for upgrading charging stations to manage increased power demand, which is essential for informed decision-making.

In this work, we target these research gaps in a comprehensive assessment of the impacts of EV fast and ultrafast charging for charging stations in China. We utilize data from real-world charging sessions at representative fast-charging stations in Beijing, China to understand the behavioral patterns. Variables include station locations (residential, commercial, shopping, etc.), the number of chargers at each station, station power loads, arrival SOCs, charging times, and station occupation rates. Scenarios reflecting technological improvements are devised. Subsequently, we analyze the relationships between EV charging power and station peak loads as a function of diverse station scales and locations. For future charging stations without sufficient power capacity, we investigate two generalized solutions that can help manage the load increase: dynamic waiting for EV charging and use of energy storage. Lastly, we discuss the costs of different upgrade strategies for fast-charging stations to support ultrafast charging. We find that increased EV charging power has a limited impact on the increase in station-wide peak loads, as faster charging sessions can reduce the probability of overlap between sessions. Just a few minutes of dynamic waiting or the use of energy storage with a high power-to-energy ratio can effectively manage surges in station loads. In cases where the grid capacity is sufficient, expanding transformer capacity instead of deployment of energy storage could achieve similar aims at lower costs. The solutions proposed here are effective in dealing with the common and more challenging situations where the grid does not have sufficient capacity. Our methods and results can be further utilized to study charging infrastructure, grid impacts, advanced energy storage, and associated policymaking.

2. Model and scenarios

A holistic, data-driven framework for investigation of EV ultrafast charging is presented in Fig. 1. It consists primarily of four parts: data, behavioral characteristics (charging characteristics), solutions, and investment costs. The real-world data of EV charging activities have been collected from the National Big Data Alliance of New Energy Vehicles (NDANEV) Open Lab. Here, we utilized real-world EV charging activities at charging stations across ten districts in Beijing, China, involving a total of over 15 thousand EVs. Details on the data and preprocessing tools are presented in Appendix A Section S1. In terms of the investigation on behavioral characteristics, the dynamic operating states of existing fast-charging stations are first examined by using EV charging activities at specific charging stations. The statistical patterns of both vehicle-level parameters, such as charging power, start/end charging time, SOC, and fleet types, and charging station-level parameters, such as the station load and the number of concurrent charging EVs (NOC), are analyzed. Then, simulations for future EV and charging station activities are performed using designed scenarios and extracted real-world vehicle arrival patterns. Supported by real-world charging behavior and previous simulations, the operating states of future ultrafast charging stations are investigated statistically. For the solution section, we focus on generalized options to enable existing charging stations that do not have sufficient power capacity to satisfy future ultrafast charging demands.

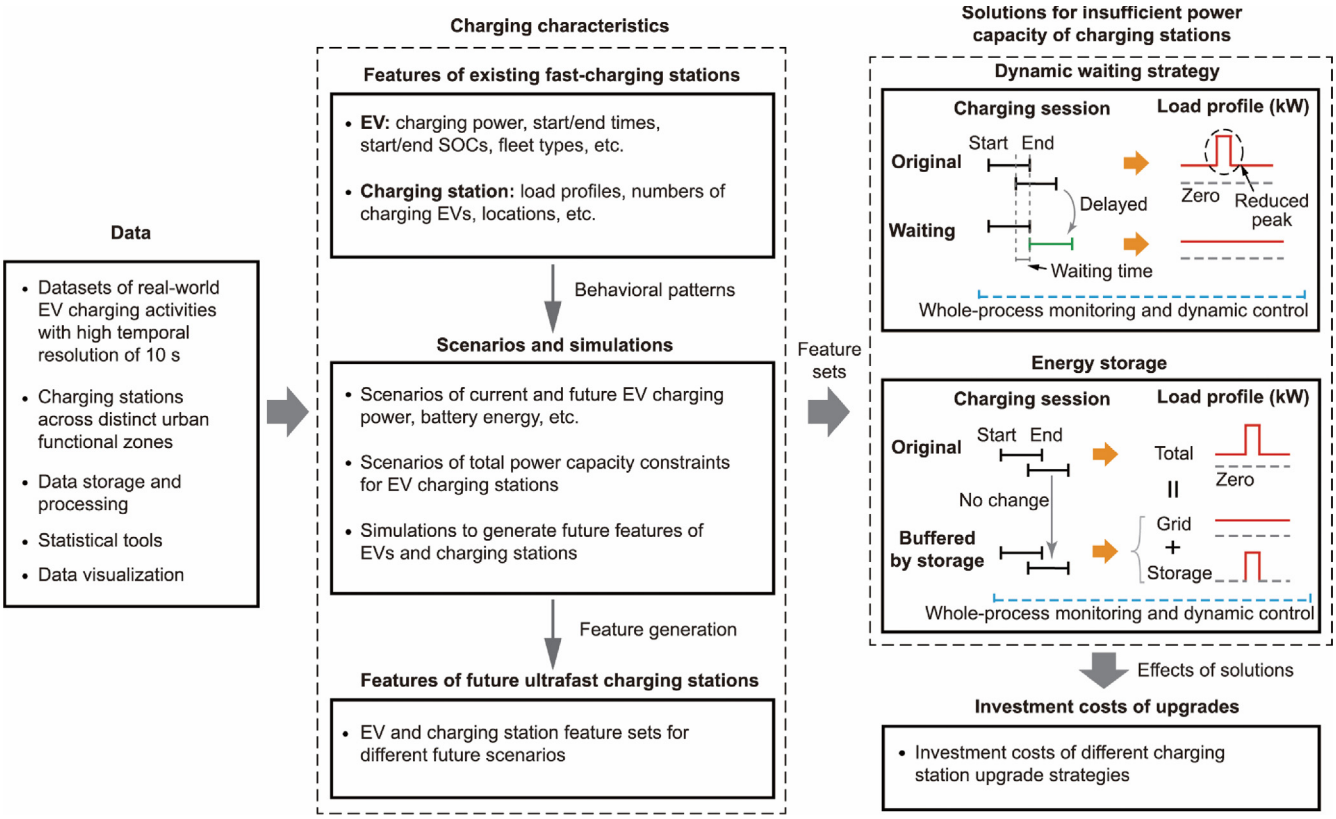

Fig. 1. Overall framework for fast and ultrafast charging station analysis.

A dynamic waiting strategy and the deployment of energy storage are evaluated. As shown, the peak shaving ability of the dynamic waiting strategy is achieved by delaying some charging sessions to reduce or eliminate their overlap. Regarding energy storage, high-power spikes can be buffered using batteries to shave peak load. For future upgrade costs, the investment cost differences between varied upgrading strategies for charging stations are compared and discussed.

We note that although this work uses real-world charging patterns, there are uncertainties in future charging behavior across different geographic regions. Charging habits could change due to local policies, costs, infrastructure availability, and climate conditions. In this work, we explore the variability among functional zones and across different days within a month to improve representativeness within the city context. We examine the sensitivity of results to a wide range of technical trends and the potential decrease in charging power induced by climate conditions. However, caution should be advised when generalizing these results to regions with low population densities, such as rural areas and along highways.

2.1. Scenarios and simulations for future EV fast and ultrafast charging

To explore future EV ultrafast charging patterns, scenarios for current and future EV specifications and charging parameters are established first. Table 1 illustrates 7 scenarios including the expected year of realization, charging power, battery energy, 20%–80% charging times, and estimated real ranges of future EVs. The parameters in the scenarios are determined according to recent literature, technical trends, and an expectation of 10-minute charging in the next decade (see Section S2 in Appendix A). Herein, scenario S1 is used to reflect the situation of recent EVs on sale while scenario S2 is used to suggest up-to-date advanced EV technologies. Note that not all fast-charging power of existing EVs is as high as 120 kW. EVs sold several years ago may only have fast-charging power of 50–100 kW. The scenarios S3, S4, and S5 scenarios are designed around expectation that most EV fleets will achieve 10-minute charging within the next decade, simulating the anticipated technological trends for this period. Scenarios S6 and S7 assume even faster technological breakthroughs in the future.

For the fast and ultrafast charging simulation, new EV charging records at the charging station are generated using both real-world charging patterns and the designated parameters in scenarios. Real-world arrival patterns (i.e., charging start times) and the distributions of initial SOCs of EVs upon arrival are employed to simulate the operating characteristics of charging stations. The performance indicators of future EVs including power- and energy-related capabilities are summarized in Table 1. Due to the excessively long time associated with the final charging stage, the end SOC is initially set at 80% to avoid conflicts with the purpose of reducing the charging time at ultrafast charging stations. Through the implementation of specific simulation procedures, new charging records including start/end times, charging power, charged energy, and start/end SOCs are obtained. Detailed procedures of the simulation and the calculation of station loads and NOCs are presented in later sections and Section S2.

2.2. Feature identification for analysis of EV charging behavior

In this work, features that can be used to reflect EV charging behavior are identified by using records of EV charging activities. To investigate charging behavior, we focus on start/end charging times, locations, EV battery states, and fleet types. The input data take the form of a daily charging activity matrix $\boldsymbol{X}^d$ on day d, which is composed of N^d charging records, each encompassing K features. They are given as follows:

Table 1
Scenarios for current and future EVs with fast or ultrafast charging capability.

Scenario	Expected year	Charging power (kW); 50% at each value	Battery energy (kW·h); 50% at each value	20% to 80% SOC charging time (min)	Estimated real range (km)
S1	2024 (existing fleet)	120, 150	90, 100	21.6–30	360–670
S2	2025	150, 250	100, 120	14.4–28.8	400–800
S3	2028	250, 350	100, 120	10.3–17.3	400–800
S4	2030	350, 550	120, 150	7.9–15.4	470–1000
S5	2035	550, 750	150, 180	7.2–11.8	590–1200
S6	2040	750, 1000	180, 200	6.5–9.6	710–1330
S7	2045	1200, 1500	200, 250	4.8–7.5	790–1670

$$\boldsymbol{X}^d = \begin{bmatrix} \boldsymbol{x}_1^d \\ \vdots \\ \boldsymbol{x}_{N^d}^d \end{bmatrix} = \begin{bmatrix} x_{1,1}^d & \cdots & x_{1,K}^d \\ \vdots & \ddots & \vdots \\ x_{N^d,1}^d & \cdots & x_{N^d,K}^d \end{bmatrix} \tag{1}$$

The vector of all the fth features, $\boldsymbol{F}^d$, is extracted by multiplying matrix $\boldsymbol{X}^d$ and an $N^d \times 1$ vector ($\boldsymbol{z}_{f=1}$) that is equal to 1 at position f and 0 at all others. The extracted features can be further filtered, aggregated, or computed according to task goals.

$$\boldsymbol{F}^d = \boldsymbol{X}^d \boldsymbol{z}_{f=1} = \begin{bmatrix} x_{1,1}^d & \cdots & x_{1,K}^d \\ \vdots & \ddots & \vdots \\ x_{N^d,1}^d & \cdots & x_{N^d,K}^d \end{bmatrix} \begin{bmatrix} 0 \\ \vdots \\ 1 \\ \vdots \\ 0 \end{bmatrix} \tag{2}$$

Charging station features such as the station load are generated by using both aggregation and computation. For instance, the charging station load L_t^d at day d and time t is calculated by summing all individual EV charging power p_i^d in kW that is not equal to 0 at the given time. Here, time t is defined as a discrete value with a resolution of 1 minute and a range of 0 to 1440 in a day. The formulation of the charging station load is given as follows:

$$L_t^d = \sum_{i \in I_t^d} p_i^d = \sum_{i=1}^{N^d} \eta(p_i^d, t) \tag{3}$$

where I_t^d is the set of indices where the charging power at time t is not equal to 0, η is a function that only returns p_i^d when the relevant charging power is greater than 0 at time t. The NOC of a charging station at time t can be calculated in the same way.

2.3. Impacts of increased EV charging power

Increasing EV charging power can not only shorten charging times but also raise charging station loads. Two aspects of the impact induced by elevated charging power are analyzed here. First, with current EV battery technologies, the final charging stage (usually the last 20%) normally cannot be implemented at the same high power as in the early charging stage. Under scenarios of increased charging power, the statistical impact of the final-charging-stage restriction on charging power and charging times is investigated using real-world EV charging data. Second, although the power of individual chargers at charging stations will increase with rising EV charging power, the shortened times of charging sessions will lower the probability of overlapping charging sessions, thereby decreasing peak loads. The overall implications of increased EV charging power on charging station loads are analyzed.

In terms of final-charging-stage restrictions, we examine the variation of the average charging power ($P_{\text{chg}}^{\text{avg}}$) and average charging duration ($T_{\text{chg}}^{\text{avg}}$) for a fleet of EVs when the charging power increases with or without a final-charging-stage restriction. P_{chg} is the charging power in kW of an EV and its potential increase is represented by C_{ra}, the ratio of P_{chg} at the raised power level to P_{chg} at its original level. For instance, in the absence of final-charging-stage restrictions, a C_{ra} value of 2 indicates that the charging power is doubled. The formulation of the average charging power is given as follows:

$$P_{\text{chg}}^{\text{avg}} = \frac{1}{N_{\text{chg}}} \sum_{i=1}^{N_{\text{chg}}} p_i^{\text{avg}} = \frac{1}{N_{\text{chg}}} \sum_{i=1}^{N_{\text{chg}}} \left[\frac{1}{N_{\text{vs}}^i} \sum_{w=1}^{N_{\text{vs}}^i} \varphi(p_w^i, \varepsilon_w^i, C_{\text{ra}}, S_{\text{fi}}) \right] \tag{4}$$

where N_{chg} defines the number of charging sessions, p_i^{avg} indicates the average charging power in kW of one modified charging session, N_{vs}^i defines the number of discrete vehicular states over time in charging session i, p_w^i and ε_w^i indicate the instantaneous charging power and battery energy state for index w, S_{fi} designates the type of final-charging-stage constraints, φ is a function that can return a modified charging power according to the ratio, constraint type, and battery energy state. Regarding S_{fi}, the final stage of charging is taken as the last 20% of SOC change, and there are three types of final-charging-stage constraints considered: a non-constrained final stage, a constrained final stage, and a dropped final stage (i.e., early termination), as explained and explored further in Section 4.

For a specific charging session i, $\bar{p}_i^{\text{ncons}}$, $\bar{p}_i^{\text{cons}}$, and $\bar{p}_i^{\text{drop}}$ indicate the average charging power for three constraint states of the final charging phase (SOC > 80%): non-constrained, constrained, and dropping of the final phase itself, respectively (discussed further in Section 4.1). They are formulated as follows:

$$\begin{bmatrix} \bar{p}_i^{\text{ncons}} \\ \bar{p}_i^{\text{cons}} \\ \bar{p}_i^{\text{drop}} \end{bmatrix} = \begin{bmatrix} \frac{1}{t_1^i + t_2^i} \left\{ \int_0^{t_1^i} C_{\text{ra}} p_i^{\text{ph1}}(t)\mathrm{d}t + \int_{t_1^i}^{t_1^i + t_2^i} C_{\text{ra}} p_i^{\text{ph2}}(t)\mathrm{d}t \right\} \\ \frac{1}{t_1^i + t_2^i} \left\{ \int_0^{t_1^i} C_{\text{ra}} p_i^{\text{ph1}}(t)\mathrm{d}t + \int_{t_1^i}^{t_1^i + t_2^i} \psi_p \left[C_{\text{ra}} p_i^{\text{ph2}}(t) \right] \mathrm{d}t \right\} \\ \frac{1}{t_1^i} \int_0^{t_1^i} C_{\text{ra}} p_i^{\text{ph1}}(t)\mathrm{d}t \end{bmatrix} \tag{5}$$

where $p_i^{\text{ph1}}(t)$ and $p_i^{\text{ph2}}(t)$ are the charging power at time t for phase 1 and phase 2, respectively. The EV SOC in phase 2 is above 80% indicating the final charging stage. t_1^i and t_2^i are the duration of the two phases and ψ_p is a function that can control the charging power below a given threshold.

The average charging time ($T_{\text{chg}}^{\text{avg}}$) in hours can be calculated by dividing the charged energy (e_i^{chg}) by the average charging power (p_i^{avg}) of a specific session i. That is,

$$T_{\mathrm{chg}}^{\mathrm{avg}}=\frac{1}{N_{\mathrm{chg}}}\sum_{i=1}^{N_{\mathrm{chg}}}\left(\frac{e_i^{\mathrm{chg}}}{p_i^{\mathrm{avg}}}\right) \tag{6}$$

2.4. Constraints for station power capacity

We analyze the capability of existing fast-charging stations to satisfy ultrafast charging demands of EVs. To that end, the power constraints that can reflect the upper limit of existing charging stations are defined and used. In 2023, the fast-charging power of existing EVs ranges normally from 50–150 kW with only a few EV models extending above 200 kW. However, the goal of ultrafast charging is to recharge the bulk of the battery energy (such as from 20% to 80% SOC) within 10 minutes. In this regard, the power of ultrafast charging needs to be as high as 350–750 kW depending on battery sizes and vehicle types. To reflect the power limit of existing charging stations, the constraints for the total charging power provided by a charging station are summarized in Table 2. In China, the average power of existing chargers at charging stations is around 60 kW and newly constructed stations reach 120 kW. Based on this, two types of constraints are employed in the analysis, and the upper limit of the total charging power at a charging station is calculated by multiplying the number of chargers by the upper power limit of an individual charger. For instance, if a charging station has 20 available chargers, the upper limit for the potential total charging power is equal to 1200 kW for constraint 1 (C1) and 2400 kW for constraint 2 (C2).

2.5. Generalized solutions to insufficient station power capacity

We adopt two types of solutions that can be generally utilized for various charging stations to address the situation of insufficient total power capacity. They include a dynamic waiting strategy and deployment of energy storage. Implementation of the waiting strategy is based on monitoring the whole process and dynamic control. Its basic functionality is achieved by the following steps: ① New arrivals are added to a waiting list in order of their arrival; and ② readiness of the station to charge each vehicle in turn on the list is decided based on the existing load states and maximum load constraints of the station. Any charging sessions that would increase the load beyond the constraint will be delayed and thus the load curve is kept below the station maximum. The dynamic control of the energy storage mainly encompasses the following steps: ① monitoring the operating states of the charging station and the energy storage; ② recognizing high-power periods (above the constraint) and low-power periods (below the constraint) of the station to ensure that the energy storage system is ready to accommodate discharge and charge, respectively; and ③ determining whether the storage system should or should not operate based on the load states and load constraints of the station as well as the energy and power state of the storage system. The high-power charging demand will be satisfied by a combination of grid power and storage system power. The optimization of energy storage parameters is described in the next section. Detailed procedures of these two generalized solutions are presented in Section S3 in Appendix A.

Table 2
Constraints for charging station loads.

Constraint	Description	Upper limit of single charger power (kW)	Upper limit of station total charging power (kW)
C1	General situation of existing fast-charging stations	60	$60 \times N_{\mathrm{m},x}^{\mathrm{org}}$
C2	Typical situation of newly built fast-charging stations	120	$120 \times N_{\mathrm{m},x}^{\mathrm{org}}$

$N_{\mathrm{m},x}^{\mathrm{org}}$ is the total number of originally available chargers (maximum of original NOCs) at charging station x.

2.6. Optimization of energy storage parameters

The parameters of the energy storage system need to be optimized to improve cost-effectiveness while maintaining the functionality of the overall charging system. The parameters of an energy storage system include the maximum energy capacity, maximum discharge/charge rates, and minimal operating energy. Provided that the peak reduction requirement can be met, a lower capacity of storage can help save investment costs. Therefore, the parameter optimization assumes a minimization of the maximum energy deployed in the energy storage system, at the same time subjecting the system to the constraints required to maintain regular operation. The equation of the optimal energy capacity, $\widehat{E}_{\mathrm{st}}^{\mathrm{opt}}$, in kW·h is given below:

$$\widehat{E}_{\mathrm{st}}^{\mathrm{opt}}=\mathrm{minimize}\chi\left(\boldsymbol{L}^{\mathrm{prov}},\boldsymbol{E}_{\mathrm{st}}^{\mathrm{max}},R_{\mathrm{st}},P_{\mathrm{st}}^{\mathrm{gate}},E_{\mathrm{min}}^{\mathrm{st}}\right) \tag{7}$$

where $\boldsymbol{L}^{\mathrm{prov}}$ is an array of charging station power that need to be provided to EVs, $\boldsymbol{E}_{\mathrm{st}}^{\mathrm{max}}$ is an array of the available values of maximum energy capacity for storage, R_{st} is the maximum discharge/charge current rate of the storage, $P_{\mathrm{st}}^{\mathrm{gate}}$ is the power threshold that determines the operation of the storage and is equal to the power constraint of the station, $E_{\mathrm{min}}^{\mathrm{st}}$ is the minimal storage energy available during operation, and χ is a function that identifies the value of the utilized maximum storage energy.

3. EV charging characteristics at fast-charging stations

This section investigates the existing and projected charging characteristics of multiple representative fast-charging stations in China. To understand the dynamic power demands of typical fast-charging stations, we look first at the real-world load and NOC profiles of five fast-charging stations in distinct urban functional zones: residential, commercial, shopping, industrial, and airports. Subsequently, EV charging activities at different charging stations are analyzed statistically to reflect the patterns of charging behavior. To study the charging patterns for future ultrafast charging stations, ultrafast charging activities are then simulated based on existing real-world charging preferences and studied under the various scenarios.

3.1. Load and NOC profiles of existing fast-charging stations

Fig. 2 displays the daily load profiles, daily NOC profiles, proportions of fleet types, and distributions of charging times across 5 representative fast-charging stations with different scales and locations. The 5 charging stations are located at the 5 zones listed above, respectively. The fleet types are distinguished for each record and 4 fleet types are included, encompassing private EVs and public EVs (i.e., fleet light-duty vehicles such as taxis, corporate cars, and rental cars). The patterns of the load profiles differ for the five charging stations. Typically, the shapes of charging station load profiles are determined by the distribution of arrival times, charging power, and charging times (duration). In Figs. 2 (b), (f), (j), (n), and (r), the NOC profiles demonstrate the traffic intensity of charging stations, with the increase in NOCs signifying new arrivals. The undulating patterns between NOC and load curves coincide, which suggests a decisive role for arrival patterns in altering the shape of the load profile.

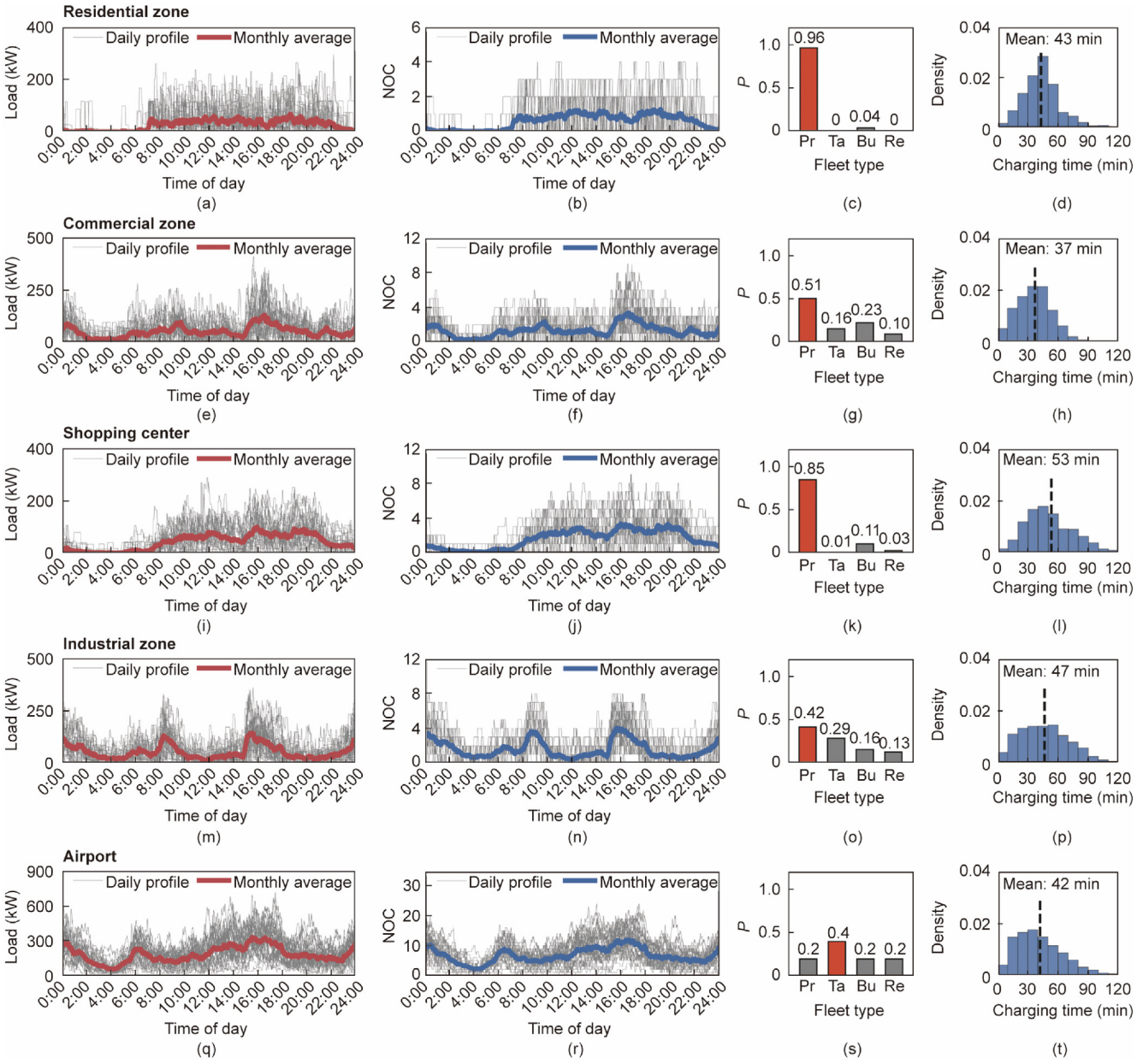

Fig. 2. Real-world charging characteristics of five representative fast-charging stations in China: (a–d) residential zone; (e–h) commercial zone; (i–l) shopping center; (m–p) industrial zone; and (q–t) airport. For load and NOC profiles, the daily curves of 30 days are presented. The maximum NOCs are 4, 9, 9, 8, and 24 for the 5 sites (top to bottom). For fleet types, the average proportions over 30 days of 4 fleet types are illustrated: private (Pr), taxi (Ta), business (Bu), and rental (Re) vehicle fleets. For charging duration, the distributions of charging times for different stations are shown.

Fleet types are incorporated to explore patterns. As shown in Figs. 2(c), (g), (k), (o), and (s), the charging stations in the residential zone and shopping center include high proportions of charging by private EVs. Comparing the load profiles of zones with high and low charging shares of private EVs shows that they are less likely to cause nighttime (23:00–6:00) high-power loads at public fast-charging stations, while public EVs are more likely to do so. Home charging is preferred for private EVs at night. As shown in Figs. 2(e), (m), and (q), the load during 15:00–17:00 rises for charging stations with high proportions of public EVs. Since daily driving distances of public EVs are typically much higher than those of private EVs, afternoon recharging is commonly used to serve the higher energy demands of the public vehicles.

The timing and duration of EV charging activities need to suit the purpose and convenience of EV users. The accessibility of charging stations is largely determined by locations. In this regard, charging stations at varied locations reflect records of distinct fleet type proportions and different shapes of load profiles. Although load patterns are different for different stations, the distributions of charging durations for the five stations considered here are similar and the average is around 44 minutes. Improvements in fast-charging technology will further reduce charging times.

3.2. Statistical analysis of charging patterns

Fig. 3(a) compares the daily average loads versus peak loads at charging stations across the five representative zones over a month. The peak loads divided by total charger numbers for the five stations are shown in Fig. 3(a) inset. Among the five sites, the airport station experiences the highest charging load (the

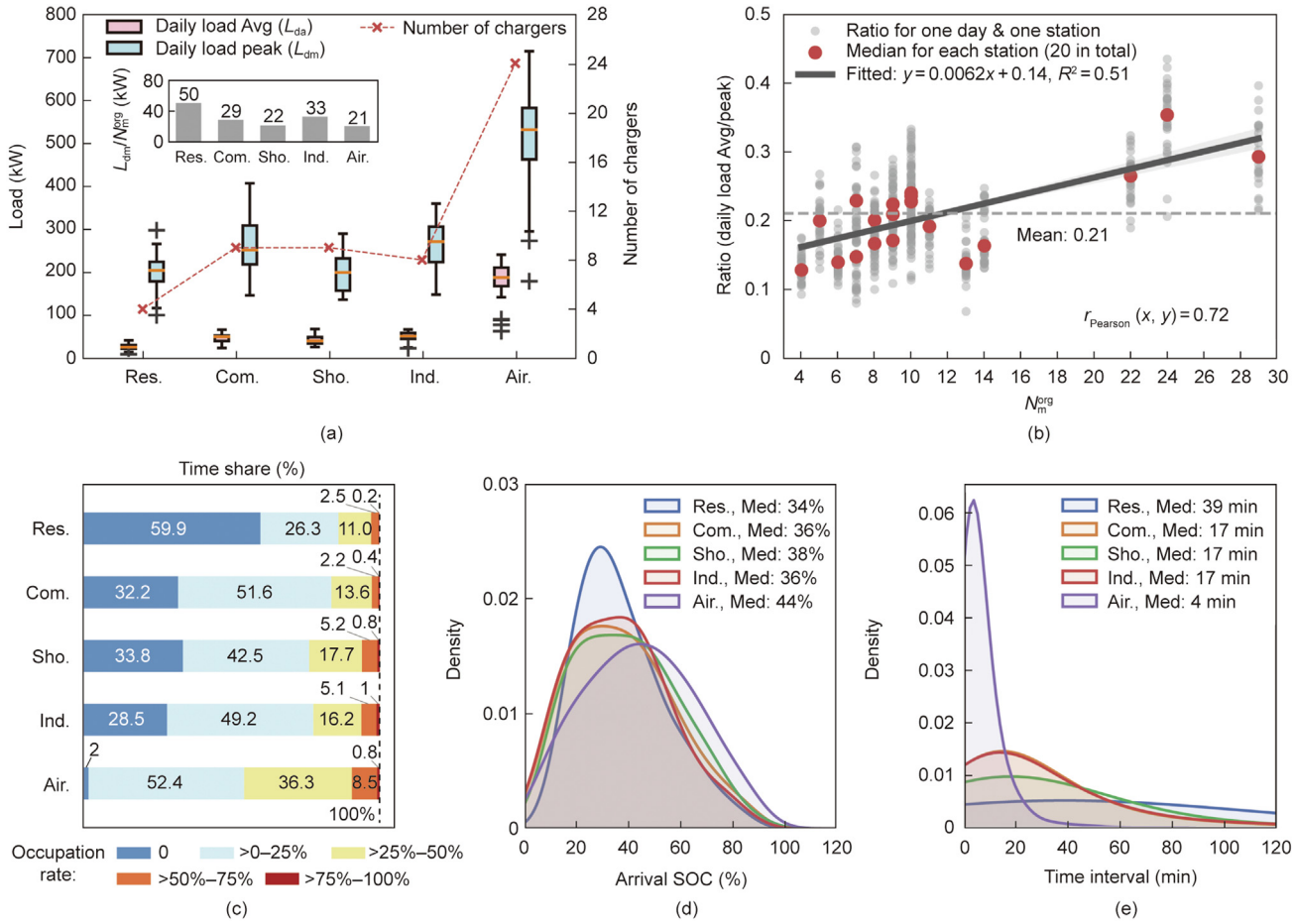

Fig. 3. Behavioral patterns of EV charging activities across different charging stations. (a) The daily average and peak loads as well as the charger number for 5 charging stations. The inset is the average peak load per charger for 5 sites. The 5 stations are located at the 5 zones: residential zone (Res.), commercial zone (Com.), shopping center (Sho.), industrial zone (Ind.), and airport (Air.). N_m^{org} indicates the number of originally available chargers in a station. (b) The ratio of the daily average load to the peak load versus the charger number for each charging station. Twenty charging stations are included. (c) Time shares of different occupation rates for 5 charging stations. The occupation rate refers to the percentage of the charging EV number to the total charger number. (d) The distributions of EV arrival SOCs for varied charging stations. (e) The distributions of the time interval between adjacent charging sessions for 5 sites. Avg: average; Med: median; R^2: coefficient of determination.

average daily peak over a month is approximately 500 kW), in large part because it has the most chargers (i.e., 24). However, the airport facility achieves the lowest average peak power per charger of 21 kW, significantly lower than that for the residential station (50 kW per charger) with only four available chargers. Fig. 3(b) compares the ratio of the daily average to the daily peak for different charging stations. The ratio has a roughly positive linear correlation with the number of chargers for each charging station; the Pearson correlation coefficient ($r_{Pearson}$) of the two variables is 0.72. Even though the mean of the average-to-peak ratio is only 0.21, a larger charging station may tend to have a higher ratio of the average load to the peak load. Fig. 3(c) displays the time shares of different occupation rates across the five charging stations. Note that 90.7% of the time collectively across the five stations features occupation rates of less than 50%, and the residential station is entirely inactive 59.9% of the time. This indicates that high occupation rates and high load states of charging stations occur only over very short periods of time.

To understand the battery levels when users start charging EVs, we investigate the distributions of arrival SOCs for EVs at the five stations as shown in Fig. 3(d). Even though the five stations have distinct scales and locations, the arrival SOC distributions are not significantly different, with medians ranging from 34% to 44%. Note that the share drops sharply at SOCs below 20%, suggesting vigilant avoidance of low battery levels. Fig. 3(e) compares the distributions of the time intervals between completed and newly initiated charging sessions for the five stations, reflecting the frequency of arrivals. The median time intervals for the airport and residential stations are 4 and 39 minutes, respectively. This illustrates that arrivals at the airport charging station are more frequent. Note that the frequency of arrivals at a charging station can also be affected by many factors such as the location, weekdays vs weekend days, electricity prices and charging fees, weather conditions, and service quality.

3.3. Ultrafast charging simulation and load estimation

In this work, 7 scenarios (see Table 1) with real-world arrival patterns are used for ultrafast charging simulations to analyze future operating states of charging stations. To illustrate the evolution from existing fast charging to future ultrafast charging, the daily profiles of the airport charging station are contrasted for four scenarios (S1, S3, S5, and S7) in Fig. 4. By comparing Figs. 4(a)–(d), the load profiles under higher charging power are more discrete (the EV charging power rises from scenarios S1 to S7, as shown in Table 1). This is because although the arrival patterns for the various scenarios are set to be identical, shorter charging times can significantly reduce session overlaps. From scenarios S1 to S7, the maximum EV charging power rises tenfold (from 150 to 1500 kW), but the peak load increases by only a factor of 4.90

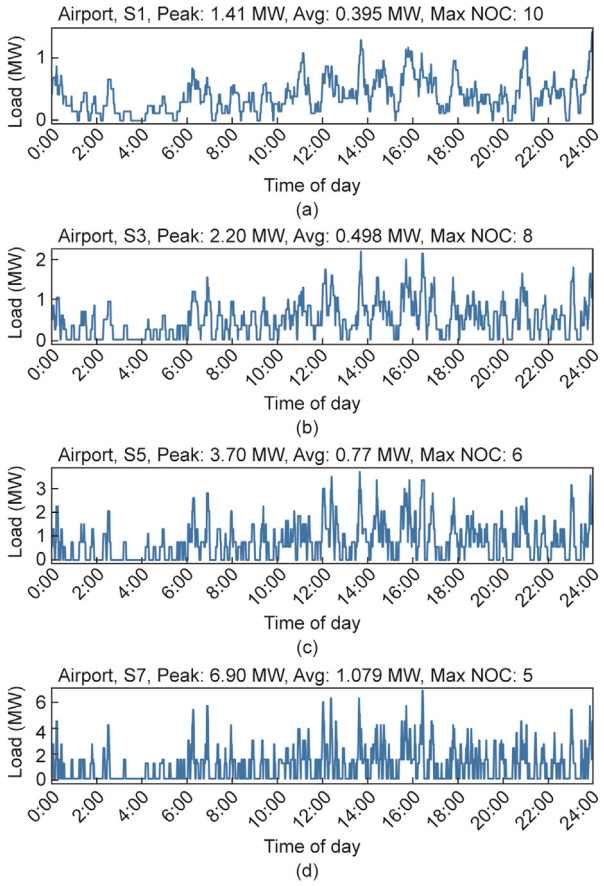

Fig. 4. Daily load profiles of a charging station for different scenarios. (a–d) are the daily profiles for scenarios S1, S3, S5, and S7, respectively.

(from 1.41 to 6.90 MW). This indicates inconsistent increases of EV charging power and charging station loads, which is examined further in the next section.

To investigate future peak loads, the monthly peak loads and average/peak (Avg/peak) ratios are depicted for the 5 charging stations across the 7 scenarios in Table 3. For all five charging stations, the peak load increases 5–7 times from S1 to S7 but the Avg/peak ratios decrease to 23.1%–30.7% of their original values. Since the arrival patterns are fixed across scenarios, the decreasing trend of Avg/peak ratios indicates that more load spikes and lower load averages occur as the scenarios move further into future ultrafast charging capabilities. Importantly, higher peaks of charging loads not only raise the costs of distribution transformers and cables in charging stations but also negatively impact the power grid. In this context, strategies to shave peaks of the EV charging load might become essential for ultrafast charging stations of the future.

4. Impact of increasing EV charging power

In this section, we analyze the increase in EV charging power and quantify its impact on charging station loads. First, we study the average power and overall duration of charging sessions considering the increase in charging power and different approaches for handling the final charging stage (SOC > 80%). Next, we evaluate the impact of increasing EV charging power on the charging station load. Real-world charging data are used to depict the typical charging behavior at fast-charging stations in China. We utilize the ratio of raised to original EV charging power (P_{chg}), defined earlier as C_{ra}, to indicate the increase in EV charging power.

4.1. Changes in average power and overall duration of charging sessions

In EV charging events, the overall charging duration is determined mainly by the average power. However, the average power of a charging session can be influenced significantly by its final charging stage (SOC > 80%). This is because current EVs store energy using lithium-ion batteries, for which the permitted maximum power in the final charging stage is usually limited. As battery technology develops, it is uncertain how future batteries will be controlled during the final charging stage, that is, to what extent such limits will apply. To explore this, three types of constraints on the final-stage power are considered: ① non-constrained; ② constrained (with a maximum power of 50 kW); and ③ early termination (charging stops at 80% SOC). Accordingly, we examine the combined effects of increased charging power and varied final-charging-stage constraints on the average power and the overall duration of charging sessions.

Fig. 5(a) shows the average charging power of an EV fleet as a function of the increasing ratio C_{ra} (the ratio of raised to original charging power). The average charging power of the light-duty EVs in this fleet is approximately 30 kW. If the final-charging-stage power is unconstrained, the average power rises at the same increase rate as C_{ra}. However, when the final-charging-stage power is constrained, average charging power grows nonlinearly at a lower rate with C_{ra} as compared with the non-constrained case. This is because the limited final-charging-stage power leads to a decrease in the overall average of the whole charging process, and the increase in EV charging power exacerbates this effect. If

Table 3
Monthly peak and average loads of 5 charging stations for 7 future scenarios.

Charging station	S1	S2	S3	S4	S5	S6	S7
Residential							
Peak	420	650	850	1100	1650	2000	3000
Avg/peak	7.8%	5.5%	4.4%	3.6%	2.7%	2.4%	1.8%
Commercial							
Peak	930	1200	1800	2000	2800	3750	5700
Avg/peak	9.3%	7.8%	5.4%	5.2%	4.1%	3.4%	2.5%
Shopping							
Peak	810	1200	1550	2000	2600	3500	5400
Avg/peak	8.6%	6.3%	5.0%	4.2%	3.5%	2.9%	2.1%
Industrial							
Peak	1110	1600	1900	2550	3350	4500	5700
Avg/peak	7.8%	5.8%	5.0%	4.1%	3.4%	2.8%	2.4%
Airport							
Peak	2040	2300	3150	4100	6100	8250	12900
Avg/peak	17.1%	16.4%	12.4%	10.3%	7.6%	6.2%	4.4%

The unit for both average and peak power is kW. The ratio (Avg/peak) is the average over peak loads in the form of percentage.

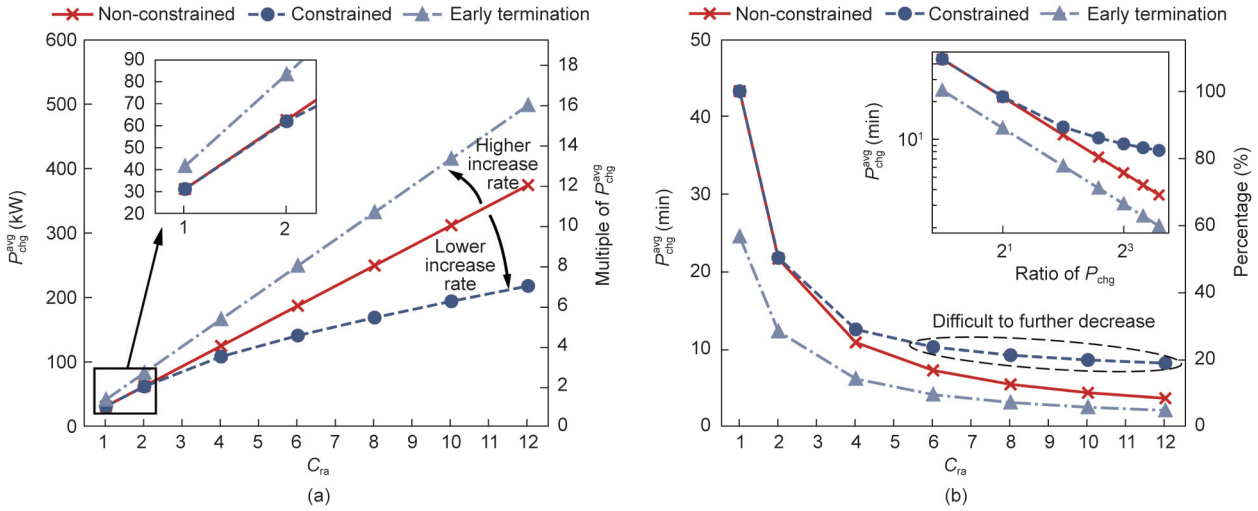

Fig. 5. Changes in average charging power and duration with increased EV charging power and varied final-charging-stage constraints. C_{ra} indicates the ratio of raised to original EV charging powers. (a) shows the average charging power of numerous light-duty EV charging sessions resulting at different C_{ra}. (b) shows the average charging duration T_{chg}^{avg} of EVs resulting at different C_{ra}. Note that further decreases in T_{chg}^{avg} above C_{ra} = 6 in the constrained case would be difficult.

charging ends at an SOC of 80% (early termination), the average power starts at ~40 kW and increases 33% faster with C_{ra} than that of the non-constrained case. This phenomenon is explained by the following equation,

$$\frac{P_{chg}^{avg,drop}}{C_{ra}} - \frac{P_{chg}^{avg,ncons}}{C_{ra}} = \frac{1}{N_{chg}} \sum_{i=1}^{N_{chg}} \left\{ \frac{t_2^i \left(\bar{p}_i^{ph1} - \bar{p}_i^{ph2} \right)}{t_1^i + t_2^i} \right\} > 0 \tag{8}$$

where $P_{chg}^{avg,drop}$ and $P_{chg}^{avg,ncons}$ denote the average charging power of the early termination and non-constrained cases, respectively; N_{chg} defines the number of charging sessions; $\bar{p}_i^{ph1}$ and $\bar{p}_i^{ph2}$ are the average power in the early charging phase (SOC ≤ 80%) and final charging phase (SOC > 80%), respectively; t_1^i and t_2^i are the duration of the two phases. Since the charging power in the early phase is greater than that in the final phase ($\bar{p}_i^{ph1} > \bar{p}_i^{ph2}$), the gradient ($P_{chg}^{avg,drop}/C_{ra}$) of the early termination case is greater than ($P_{chg}^{avg,ncons}/C_{ra}$) for the non-constrained case. Detailed mathematical processes are described in Section S4 in Appendix A.

Fig. 5(b) shows the decrease in average charging duration for charging activities versus the increasing C_{ra} of EV charging power. Since real-world charging activities usually start from an SOC of 30%–40% as mentioned earlier, completing a charging session within 10 minutes does not always need extremely high power. As shown, to reduce the average charging duration to 10 minutes for the EV fleet, the average charging power needs to be increased by a factor of 3 (~120 kW) with an 80%-SOC termination. However, for conditions with a final-charging-stage power constraint, the peak power needs to increase by a factor of 8 (~240 kW), and in this case, it is difficult to accommodate a continuing reduction in charging duration. These results demonstrate the value of control of final-charging-stage power in accommodating a future reduction in EV charging times.

4.2. Impact of increased EV charging power on station loads

It is commonly assumed that doubling the charging power of EVs in a charging station will inherently double the charging station load. Often overlooked is that increasing charging power will also shorten charging durations and thus reduce overlap of charging sessions. To quantify the impact of increasing EV charging power on station operations, we simulate the power increase in charging activities at stations based on real-world data from representative fast-charging stations. The final-charging-stage constraint here is set at early termination (charging stops at 80% SOC). Multiple variables are considered including the ratio of EV charging power, daily peak loads, the maximum number of available chargers at a charging station, and the daily peak number of available chargers. To better represent the general patterns, all of the daily peak values employed in this section are averaged over thirty-day intervals.

Fig. 6(a) depicts the relationship between the ratio of raised to original EV charging power (C_{ra}) and the daily peak load (L_{dm}). The peak load increases with the increase in EV charging power. We normalize the peak load to the ratio of successive values to the original value (i.e., C_{ra} = 1), to compare the rates of increase between types of stations. It can be seen from Fig. 6(b) that the rates of increase for all curves are lower than $y = x$, that is, a doubling of EV charging power yields a less than doubled increase in peak load.

It is noteworthy that the rate of increase in the peak load for the residential station is clearly higher than that for the airport station. To better understand this, we incorporate charging station scales into the analysis. Fig. 6(c) illustrates the rate of increase of peak loads (reflected by the gradient k of the lines in Fig. 6(b)) as a function of the number of available chargers (N_m^{org}) for each charging station. The gradient is calculated by

$$\boldsymbol{w} = \text{argmin}_{\boldsymbol{w}} \|\boldsymbol{X}\boldsymbol{w} - \boldsymbol{y}\|_2^2 \tag{9}$$

where $\boldsymbol{w}$ is $[k, b]^T$, $\boldsymbol{y}$ is the vector of the ratio of L_{dm}. $\boldsymbol{X}$ contains two columns where the first is C_{ra} and the second is a vector of ones, and argmin is a function to find the values in $\boldsymbol{w}$ that minimize the argument. The rate of increase of k decreases almost linearly (R^2 = 0.73) with the number of available chargers. This means that increasing EV charging power has a lower impact on raising the charging load for locations with more available chargers. Doubling EV charging power only raises the load by 20%–60% for different charging stations.

We quantify the influence of increased EV charging power on reducing charging session overlap. Fig. 6(d) shows the daily peak

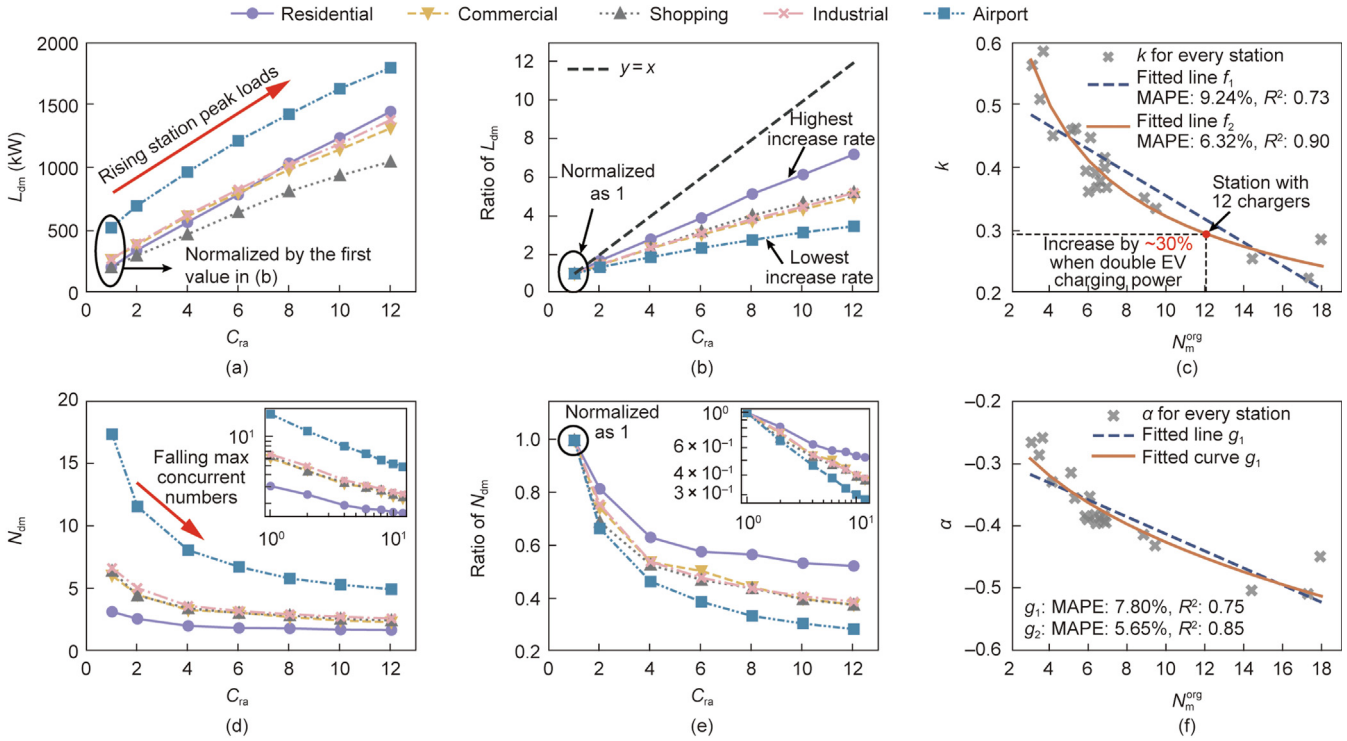

Fig. 6. Relationship between increasing EV charging power and station peak loads. C_{ra} indicates the the ratio of increased to original EV charging powers. (a) The daily charging station peak load L_{dm} versus C_{ra}. (b) The ratio of L_{dm} with C_{ra}. The ratio of L_{dm} is calculated by dividing each value by the first value. (c) The gradient k versus the number (N_m^{org}) of original available chargers at a charging station. k is the gradient of the lines in (b). MAPE: mean absolute percentage error. (d) The daily peak number (N_{dm}) of concurrent charging EVs versus C_{ra}. (e) The ratio of N_{dm} with C_{ra}. The ratio of N_{dm} is calculated by dividing each value by the first value; the inset is obtained by logarithmic conversion. (f) The gradient α versus N_m^{org}. α is the gradient of the lines in the inset in (e).

number (N_{dm}) of concurrently charging EVs with C_{ra}. The results in Fig. 6(d) are normalized by dividing by their respective original values, as shown in Fig. 6(e). We find that the daily peak number decreases significantly with the increase in charging power but with different rates of decrease across different charging stations. Fig. 6(f) shows the gradient α of the log-transformed curves in Fig. 6(e) inset versus the number of available chargers N_{dm}^{org}. The calculation of the gradient α is similar to that for the gradient k in Fig. 6(c) but with an additional logarithmic transformation for the input. Since the gradients are negative, smaller ones indicate higher rates of decrease of N_{dm}. Combining the results, we can infer that greater availability of chargers provides more capacity to reduce the number of concurrent active chargers when the EV charging power rises, in turn reducing the chance of session overlap. From the linear results, doubling EV charging power causes a modest marginal increase of less than 30% in peak loads for stations with 12 chargers or more, and less than 40% for those with more than 8. Overall, the results suggest that increasing EV charging power will decrease the number of concurrent active chargers, helping to explain peak load increases of only 20%–60% in response to a doubling of EV charging power. Stations with more available charging spots yield a smaller increase rate of the station peak load with the increase of EV charging power.

To analyze sensitivity to future technological trends, we also include 14 additional scenarios in Section S4, each featuring single values for charging power (150–1500 kW) and battery energy (100–250 kW·h). We simulate the impact of potential charging power reductions due to low winter temperatures using two settings (–20% and –50%). As preheating of batteries is common in current EVs, reductions in battery energy are not emphasized. We found that increasing battery energy at a given power level elevates station peak power only when the number of charging EVs at peak times rises. Additionally, reductions in charging power due to low temperatures generally decrease station peak power; however, they can also maintain or even increase peak power when slower charging leads to significant overlap in charging sessions.

5. Implications of constrained grid interaction for ultrafast charging stations

In this section, we use two generalized solutions to examine the ability of existing fast-charging stations to satisfy the loads of future ultrafast charging stations. To that end, ultrafast charging simulations and real-world charging patterns are leveraged first to generate high-power charging records for the 7 scenarios (S1–S7, see Table 1) reflecting technological progress in terms of rising charging power from 120 to 1500 kW. Two thresholds for the total power capacity of stations (at an average of 60 or 120 kW for each charger, per the C1 and C2 cases of Table 2) are used to constrain the grid interaction of charging stations. Two types of generalized solutions are incorporated that can mitigate the peak load, that is, a dynamic waiting strategy and use of energy storage.

5.1. Dynamic waiting strategy

A dynamic waiting strategy, managed by the system, would decrease peak loads by delaying the starting times for some charging sessions. Accordingly, the peak number of concurrent active chargers can be decreased. This can not only improve the ability of existing fast-charging stations to satisfy higher charging power, but also reduce the costs required for potential upgrades to ultrafast

charging. Nevertheless, a lower power capacity of a charging station or a smaller number of available chargers will inevitably prolong the waiting times for EVs. To test the effectiveness, we apply the dynamic waiting strategy to investigate charging records under the 7 scenarios. Three charging stations (residential, commercial, and airport) with different sizes are selected.

Figs. 7(a)–(c) illustrate the average and maximum waiting times across 7 scenarios for charging stations near residential areas, commercial areas, and an airport, respectively, under the two station power constraints C1 and C2. To visualize reduced overlap of charging sessions, the number of concurrent charging EVs is computed, with the maximum NOC shown in Figs. 7(d)–(f). The numbers of available chargers (N_m^{org}) at these three stations are 4, 9, and 24, as given in Figs. 7(d)–(f). Note that a result is not given if the total charging power is insufficient to charge even one EV or if the maximum waiting time exceeds 60 minutes.

It is noteworthy that if a total power capacity of 120 kW (under C2) times the charger number is provided, the airport EV charging station can satisfy the ultrafast charging demands from S1 to S7 by using only the dynamic waiting strategy. In this case, from S1 to S7, the average and maximum waiting times increase from 0 to 2.1 minutes and from 0 to 41 minutes, respectively; the maximum concurrent charging number falls from 17 to 2. If the power capacity is decreased to 60 kW (under C1) times the number of charging ports, the airport EV charging station can only satisfy the demand from S1 to S4.

By comparing the results across three charging stations, we find that stations with more chargers can serve the charging demands of more scenarios. Two reasons explain this: ① Charging stations with more chargers usually have a higher total power capacity, which helps deal with high-power charging; and ② more chargers can handle more charging sessions and thus provide more flexibility for dynamic adjustments. An unusual situation is that of the commercial charging station, in which the average waiting time of S6 is shorter than that of S5 (lower power and energy demands than S6) under the C2 constraint. This is because a longer waiting time is required to respond to the decrease in the number of available chargers. However, the charging station can only afford to charge one EV in both scenarios above (see results of S5 and S6 in Fig. 7(e)). Thus, the average waiting time is shortened with increasing EV charging power.

The results for more charging stations are presented in Section S5 in Appendix A. Under various scenarios, the average waiting time at different stations is only a few minutes. For fast-charging stations with around 9 chargers (average 120 kW per charger), the average waiting time for scenario S4 (charging power of 350–550 kW, battery energy of 120–150 kW·h) is less than 1 minute, and the maximum waiting time is less than 20 minutes. As the average of 20% to 80% SOC active charging times for scenario S4 is around 12 minutes (Table 1), the estimated average overall 20% to 80% charging time (waiting plus active charging) is approximately 13 minutes. As described previously, however, the arrival SOC of EVs ranges from 34%–44%, so the more common overall time from the start of charging to 80% will be approximately 9 minutes (including 1 minute of waiting).

5.2. Energy storage with dynamic control

Energy storage provides a buffer against charging station peak loads by dynamically providing extra power and energy. Different from the waiting strategy, the use of energy storage does not affect the charging behavior of EVs but requires investments in necessary storage and related devices. A question is whether future demand for ultrafast charging can be satisfied by adding energy storage to existing charging stations. In the absence of limits on power and energy limits on storage devices, fully

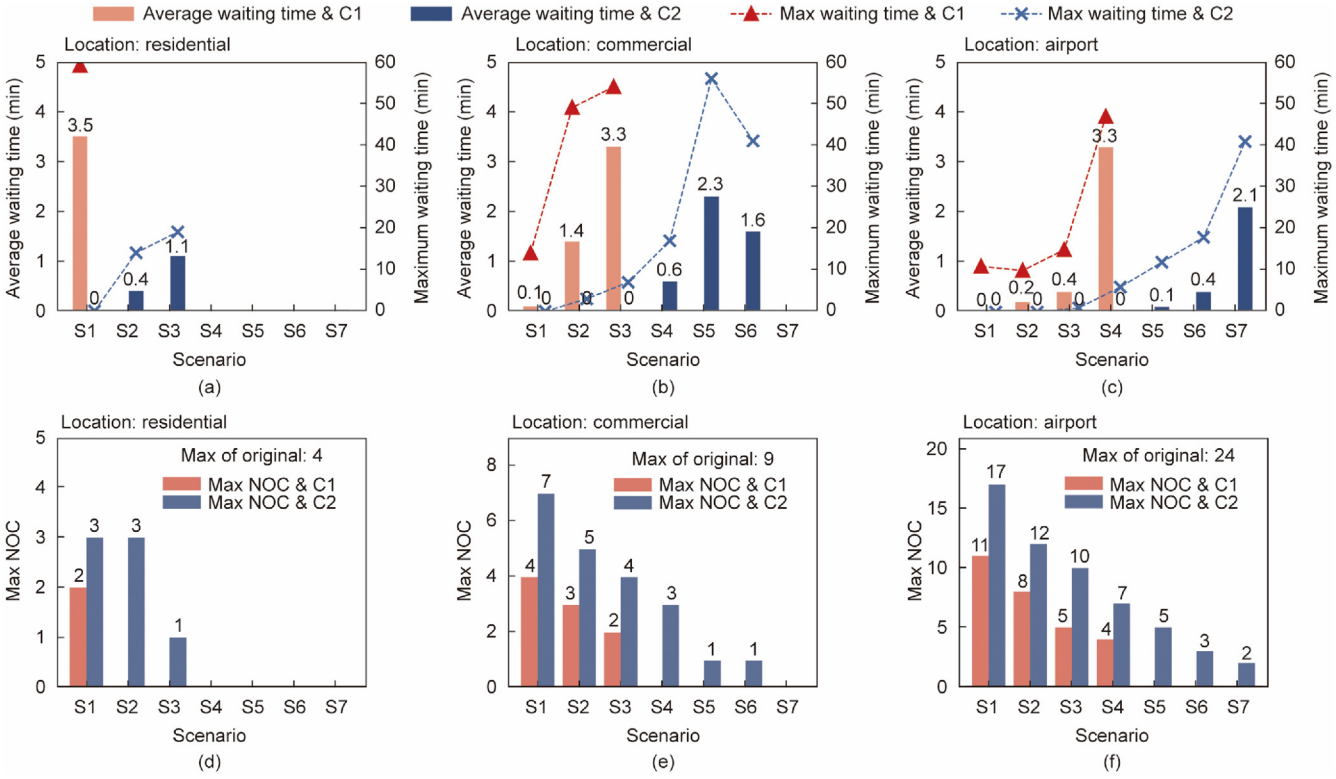

Fig. 7. Effects of dynamic waiting strategy. (a–c) show the average (bars, left *y*-axis) and maximum (symbols, right *y*-axis) waiting times under charging power constraints C1 or C2 for 3 types of charging stations in the 7 scenarios. (d–f) are the maximum number of concurrent charging EVs (max NOC) under the two constraints for the 3 charging stations in the 7 scenarios.

satisfying demand requires only that the average daily EV charging power should be lower than the power capacity of the charging station and can effectively ignore peak demand. In practice, however, the energy and power requirements for energy storage are minimized to save investment costs. Here, we examine the change in energy and power requirements for energy storage across the varied charging stations in the future scenarios. Multiple variables are considered, including charging stations with varied locations, power constraints, and maximum charge/discharge rates for energy storage.

Figs. 8(a)–(c) compare the minimized storage energy that can satisfy the future ultrafast charging demands for three types of charging stations. Three charge/discharge current rates (1C, 2C, and 3C) and the two station power constraints of Table 2 (C1 and C2) are considered. First, note that adequate energy storage would allow all three fast-charging stations to meet the ultrafast charging demands for all 7 scenarios, even if the total power capacity is according to C1 (60 kW times the number of chargers). This is because, despite high peak power demands, the daily average EV ultrafast charging power of the station is sufficiently low. Raising the total power capacity of the station to C2 (120 kW times the number of chargers) can greatly lower requirements for energy storage in the first few scenarios.

Higher discharge/charge current rates can effectively bring down the requirement for storage energy. With a rise in the charge/discharge rate from 1C to 3C, the required energy of the storage is reduced by 61%–67% for the airport EV charging station. The marginal decrease of the required energy storage between 1C and 2C is higher than that between 2C and 3C. Further raising the discharge/charge rate beyond 3C has a limited impact on reducing

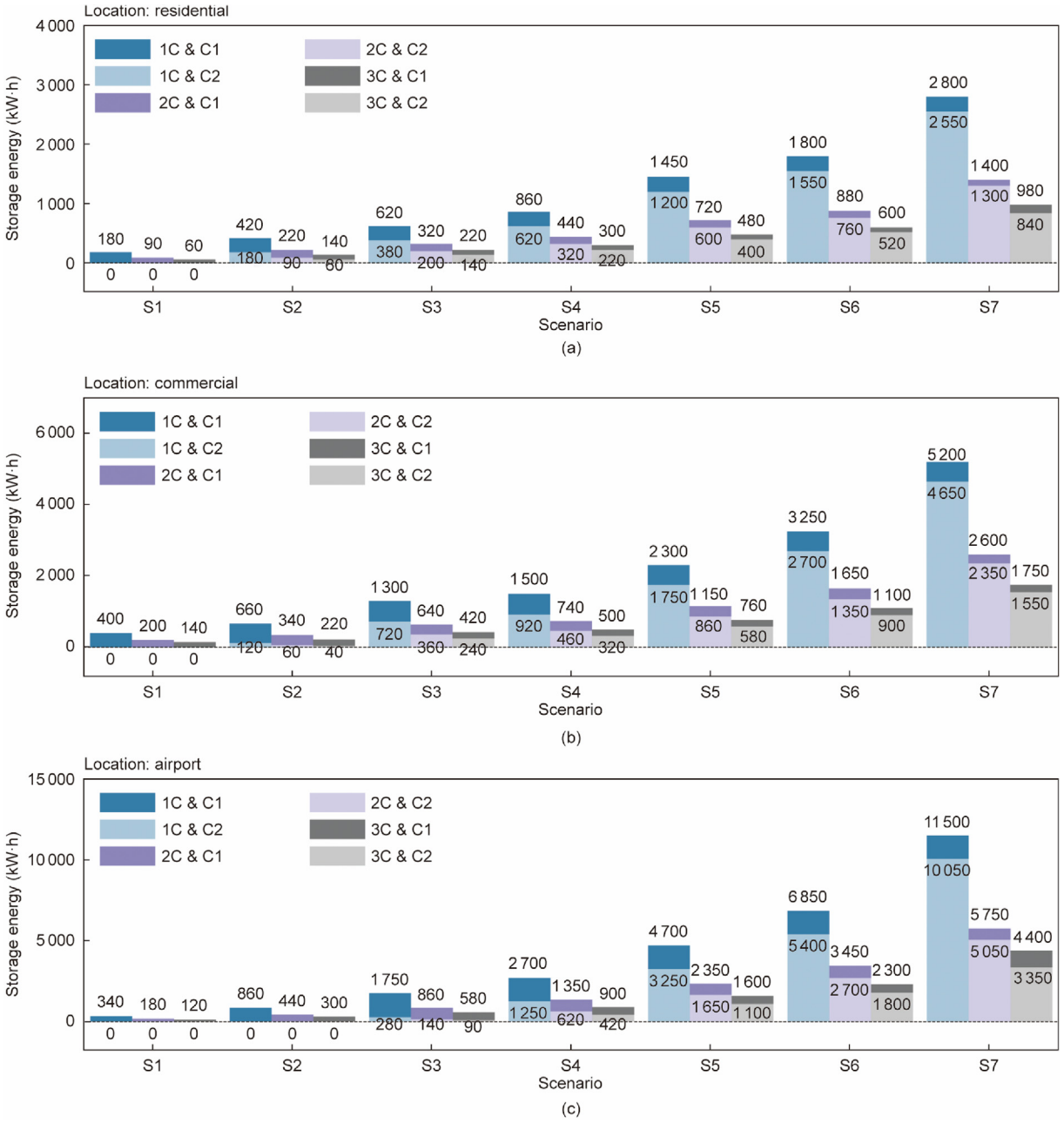

Fig. 8. Minimized storage energy for seven scenarios across three types of charging stations. (a–c) are results for three charging stations near residential areas, commercial areas, and an airport, respectively. Three charge/discharge current rates are considered: 1C, 2C, and 3C. C1 and C2 are the two charging station power constraints.

the energy capacity of storage (see Section S5). This indicates that more storage energy is used only to supply higher power when the discharge/charge rate is lower than 3C. In this regard, as long as the power requirement for energy storage (below 3C) is met, the energy demand can also be served, which helps to differentiate the predominant source of demand. In addition, the selection of appropriate energy storage is critical. A charge/discharge rate of 3C is high for commercial- and utility-scale energy storage systems where 0.5C–1C is now more common but is low for those power battery systems (e.g., in EVs) where 10C can be easily accommodated.

Since regional climate conditions can also affect EV charging efficiency, we analyze the impact of reduced charging power due to low winter temperatures on the minimum storage energy requirements. As depicted in Section S5, the required storage energy decreases as charging power decreases. For instance, in the 1C category, the minimum storage energy decreases nearly proportionally with the reduction in charging power. This occurs because EV charging patterns remain unchanged when energy storage is utilized, causing variations in charging power to be directly reflected in the station's power demand. We note that if peak power demand is higher during specific seasons, such as summer, investments in energy storage should account for worst-case scenarios to ensure reliability.

6. Investment costs of charging station upgrades

The cost of a charging station includes both initial investment costs (chargers, distribution transformers, land, construction, etc.) and operating costs (operation and maintenance, electricity, etc.). A study in 2019 [33] indicated that in China, the initial investment for a public charging station with 30 60-kW DC fast chargers amounted to approximately 0.3 million USD. Meanwhile, from data [34] for the United States in 2019, the cost of 30 50-kW DC fast chargers plus related installation costs can reach 1.38 million USD, far more than in China (see Section S6 in Appendix A). While some types of costs are high in the initial investment, such as costs for land use and initial construction, later station upgrade costs are mainly incurred due to upgrades of chargers and distribution transformers. Since the cost of upgrading chargers usually cannot be avoided, the difference in the upgrade costs across varied strategies mainly depends on how to raise station power capacity. Generalized strategies to handle high peak loads, such as using the waiting strategy and deploying energy storage, can effectively lower the need for additional transformer capacity. In this case, there is a trade-off between increasing transformer capacity and the use of alternative solutions.

We compare the cost differences across three strategies: use of the strategic waiting option, increasing transformer capacity, and deploying energy storage. For the first, the cost of using a waiting strategy is minimal compared with the other two, as it needs only the deployment of suitable control and management systems. By contrast, both transformer and energy storage options require the purchase of additional expensive devices, meaning transformers, battery energy storage, or both. For the primary device costs of the latter two strategies, the average unit cost of pad-mounted distribution transformers in China is approximately 46 USD·kVA^{-1}, and the average unit cost of lithium-ion battery energy storage systems (one-hour storage for the 1C rate) in China is approximately 196 USD·(kW·h)$^{-1}$ (see Section S6). From previous results, once the power requirement for 1C energy storage in EV charging stations is met, the energy requirement will also be met. For example, when there is a peak load increase of 1200 kW in EV charging stations, the cost of a one-hour lithium-ion battery energy storage system (1200 kW·h & 1200 kW) is 0.235 million USD, which is approximately 4 times the cost of a 1200 kVA pad-mounted distribution transformer. In this case, the unit cost of battery storage needs to decrease by 76.5% to be cost-competitive. However, if the capacity of distribution networks is insufficient, the option of increasing transformer capacity to upgrade stations will be either technically infeasible or extremely costly. In this case, reducing the number of ultrafast chargers or deploying energy storage could be more cost-effective.

7. Discussion and conclusions

This work reports an exploratory analysis of future high-power charging stations in China. We used integrated assessment models and real-world EV charging data to study the operating patterns of existing fast and potential future ultrafast charging stations. The quantitative analysis of this work yields some key conclusions.

First, we analyze the behavioral characteristics of fast-charging stations. Stations with more charging spots exhibit higher ratios of daily average-to-peak loads, indicating that larger stations are visited more frequently. High-load periods are brief, with stations operating below 50% occupancy over 90.7% of the time. In future scenarios, ultrafast charging stations are expected to experience higher peak-to-average load ratios.

Second, we investigate the impact of increased EV charging power on station power loads. Our findings suggest that greater availability of chargers in a station makes the increase in EV charging power have less impact on amplifying the station load due to less overlap of shorter charging sessions. For instance, doubling EV charging power increases station peak power by only 20% to 60%. This insight suggests that when designing EV charging stations, larger charging stations can be prioritized in high-demand areas, as they can accommodate higher-power chargers without significantly increasing peak loads, thereby reducing strain on the power grid.

Third, we assessed the solutions to grid capacity constraints on charging stations. Our results indicate that, at current fast-charging station capacities, implementing dynamic waiting strategies with an average waiting time of a few minutes or high-power energy storage ($\geq$ 3C) can effectively help manage future ultrafast charging loads.

Finally, we discussed the investment cost of various charging station upgrade strategies, identifying charging piles and distribution transformers as primary expenses. Comparing upgrade strategies, the cost per kilowatt of adding battery storage is ~4 times higher than the cost for expanding distribution transformers. Meanwhile, the battery storage option offers several benefits. For instance, it does not require grid capacity expansion, allows for more flexible installation (though space considerations may apply), and can take advantage of lower electricity rates during off-peak periods.

To meet surging charging demands of EVs in China and further support the transition to sustainable transportation, it is essential to consider deploying ultrafast charging stations in high-demand regions. This initiative will enhance charging convenience for EV users with limited home charging options and/or in populous regions. Based on the results in this work and the fact that current advanced charging technology has exceeded half a megawatt, we recommend deploying large ultrafast charging stations with chargers between 350 to 550 kW in high-demand regions immediately. Future studies can leverage the charging patterns and station load profiles presented in this work to inform charging infrastructure buildout and upgrades. The statistical relationships between EV charging power and station peak loads can be used to project future impacts on the power grid.

CRediT authorship contribution statement

Yang Zhao: Writing – original draft, Methodology, Investigation, Conceptualization. **Xinyu Chen:** Writing – review & editing, Supervision, Conceptualization. **Peng Liu:** Supervision, Data curation. **Chris P. Nielsen:** Writing – review & editing, Supervision. **Michael B. McElroy:** Writing – review & editing, Supervision.

Declaration of competing interest

The authors declare that they have no known competing financial interests or personal relationships that could have appeared to influence the work reported in this paper.

Acknowledgments

The authors acknowledge the support of the National Natural Science Foundation of China (72325006, 72488101, and 72293601), the Sze Family Foundation, and the Climate Imperative Foundation (#2024-001465).

Appendix A. Supplementary data

Supplementary data to this article can be found online at https://doi.org/10.1016/j.eng.2025.01.015.

References

[1] International Energy Agency (IEA). Global EV outlook 2024. Report. Paris: International Energy Agency; 2024.
[2] International Energy Agency (IEA). Global EV outlook 2023. Report. Paris: International Energy Agency; 2023.
[3] International Energy Agency (IEA). Global EV outlook 2022. Report. Paris: International Energy Agency; 2022.
[4] International Energy Agency (IEA). Global EV outlook 2021. Report. Paris: International Energy Agency; 2021.
[5] Zhao Y, Jiang Z, Chen X, Liu P, Peng T, Shu Z. Toward environmental sustainability: data-driven analysis of energy use patterns and load profiles for urban electric vehicle fleets. Energy 2023;285:129465.
[6] Xinhua News Agency. An increase of 49.6%! The year-on-year growth rate of EV charging facilities in the first three quarters reflects three major trends [Internet]. Beijing: Xinhua News Agency; 2024 Nov 12 [cited 2024 Dec 10]. Available from: https://www.gov.cn/lianbo/bumen/202411/content_6984504.htm. Chinese.
[7] Weiss M, Ruess R, Kasnatscheew J, Levartovsky Y, Levy NR, Minnmann P, et al. Fast charging of lithium-ion batteries: a review of materials aspects. Adv Energy Mater 2021;11(33):2101126.
[8] Li M, Feng M, Luo D, Chen Z. Fast charging li-ion batteries for a new era of electric vehicles. Cell Rep Phys Sci 2020;1(10):100212.
[9] Kang B, Ceder G. Battery materials for ultrafast charging and discharging. Nature 2009;458(7235):190–3.
[10] Lu LL, Lu YY, Zhu ZX, Shao JX, Yao HB, Wang S, et al. Extremely fast-charging lithium ion battery enabled by dual-gradient structure design. Sci Adv 2022;8(17):eabm6624.
[11] Ye L, Li X. A dynamic stability design strategy for lithium metal solid state batteries. Nature 2021;593(7858):218–22.
[12] Wang L, Qin Z, Slangen T, Bauer P, Van Wijk T. Grid impact of electric vehicle fast charging stations: trends, standards, issues and mitigation measures—an overview. IEEE Open J Power Electron 2021;2:56–74.
[13] Diandongbang. The 8 fastest charging electric vehicles, Porsche can run 400 kilometers by 15-minute charging [Internet]. Beijing: Autohome.com; 2018 Sep 19 [cited 2023 Apr 5]. Available from: https://chejiahao.autohome.com.cn/info/2757665. Chinese.
[14] Juice. The battle for ultra-fast charging of electric vehicles begins! The layout of 14 car companies, interpreting the three key points behind the technology [Internet]. Beijing: Chedongxi; 2022 Oct 22 [cited 2023 Apr 5]. Available from: https://new.qq.com/rain/a/20221011A07AUS00. Chinese.
[15] Lambert F. Tesla is deploying its first Supercharger V4, and it's huge [Internet]. Failsworth: Electrek; 2023 Mar 3 [cited 2023 Apr 4]. Available from: https://electrek.co/2023/03/03/tesla-deploying-first-supercharger-v4-huge/.
[16] Lambert F. Tesla announces 500 kW charging as it finally delivers V4 Supercharger cabinets [Internet]. Failsworth: Electrek; 2024 Nov 14 [cited 2024 Dec 15]. Available from: https://electrek.co/2024/11/14/tesla-announces-500-kw-charging-as-it-finally-delivers-v4-supercharger-cabinets/.
[17] Wilkinson S. Porsche Taycan review: range, battery & charging [Internet]. London: DrivingElectric™; 2024 Apr 4 [cited 2024 Dec 15]. Available from: https://www.drivingelectric.com/porsche/taycan/range.
[18] Lima P. GAC Aion with fast charging speed comparable to refueling [Internet]. New York City: PushEVs; 2021 Jul 30 [cited 2023 Apr 5]. Available from: https://pushevs.com/2021/07/30/gac-aion-with-fast-charging-speed-comparable-to-refueling/.
[19] Attia PM, Grover A, Jin N, Severson KA, Markov TM, Liao YH, et al. Closed-loop optimization of fast-charging protocols for batteries with machine learning. Nature 2020;578(7795):397–402.
[20] Dufek EJ, Abraham DP, Bloom I, Chen BR, Chinnam PR, Colclasure AM, et al. Developing extreme fast charge battery protocols—a review spanning materials to systems. J Power Sources 2022;526:231129.
[21] Kumar Thakur A, Sathyamurthy R, Velraj R, Saidur R, Pandey A, Ma Z, et al. A state-of-the art review on advancing battery thermal management systems for fast-charging. Appl Therm Eng 2023;226:120303.
[22] Lempert J, Kollmeyer PJ, He M, Haußmann M, Cotton JS, Emadi A. Cell selection and thermal management system design for a 5C-rate ultrafast charging battery module. J Power Sources 2022;550:232121.
[23] Tu H, Feng H, Srdic S, Lukic S. Extreme fast charging of electric vehicles: a technology overview. IEEE Trans Transp Electrif 2019;5(4):861–78.
[24] Aretxabaleta I, De Alegria IM, Andreu J, Kortabarria I, Robles E. High-voltage stations for electric vehicle fast-charging: trends, standards, charging modes and comparison of unity power-factor rectifiers. IEEE Access 2021;9:102177–94.
[25] Greater bay technology with TELD new energy to build thousands of supercharge stations [Internet]. Guangzhou Automobile Group Co., Ltd.; 2022 May 17 [cited 2023 Apr 8]. Available from: https://www.gac.com.cn/cn/news/detail?baseid=18416. Chinese.
[26] Ahmad A, Qin Z, Wijekoon T, Bauer P. An overview on medium voltage grid integration of ultra-fast charging stations: current status and future trends. IEEE Open J Ind Electron 2022;3:420–47.
[27] Meyer D, Wang J. Integrating ultra-fast charging stations within the power grids of smart cities: a review. IET Smart Grid 2018;1(1):3–10.
[28] Fang C, Lu H, Hong Y, Liu S, Chang J. Dynamic pricing for electric vehicle extreme fast charging. IEEE Trans Intell Transp Syst 2020;22(1):531–41.
[29] Liu G, Xue Y, Chinthavali MS, Tomsovic K. Optimal sizing of PV and energy storage in an electric vehicle extreme fast charging station. In: Proceedings of the 2020 IEEE Power & Energy Society Innovative Smart Grid Technologies Conference (ISGT); 2020 Oct 26–28; The Hague, Netherlands. New York City: IEEE; 2020. p. 1–5.
[30] Leone C, Peretti C, Paris A, Longo M. Photovoltaic and battery systems sizing optimization for ultra-fast charging station integration. J Energy Storage 2022;52:104995.
[31] di Noia LP, Mottola F, Proto D, Rizzo R. Real time scheduling of a microgrid equipped with ultra-fast charging stations. Energies 2022;15(3):816.
[32] Iannuzzi D, Franzese P. Ultrafast charging station for electrical vehicles: dynamic modelling, design and control strategy. Math Comput Simul 2021;184:225–43.
[33] Natural Resources Defense Council (NRDC). Analysis on developing a healthy charging service market for EVs in China. Beijing: Natural Resources Defense Council; 2019.
[34] Nicholas M. Estimating electric vehicle charging infrastructure costs across major US metropolitan areas [Internet]. Washington, DC: International Council on Clean Transportation; 2019 Aug 12 [cited 2024 Dec 15]. Available from: https://theicct.org/publication/estimating-electric-vehicle-charging-infrastructure-costs-across-major-u-s-metropolitan-areas/.